Journal Name

ARTICLE

Low-Temperature-Flux Syntheses for Ultraviolet-Transparent Borophosphates $Na_4MB_2P_3O_{13}$ (M = Rb, Cs) Exhibiting Second-Harmonic Generation Response

Received 00th January 20xx,
Accepted 00th January 20xx

DOI: 10.1039/x0xx00000x

www.rsc.org/

Chao Wu,[a,b,c] Longhua Li,[d] Junling Song,[a] Gang Yang,[a] Bing Yan,[b] Mark G. Humphrey,[b,e] Long Zhang,[c] Jianda Shao,[c] and Chi Zhang*[,a,b,c]

The first non-centrosymmetric mixed-alkali-metal borophosphates, $Na_4MB_2P_3O_{13}$ (M = Rb **1**, Cs **2**), were obtained using a low-temperature flux method. Single-crystal X-ray diffraction studies of **1** and **2** reveal that the two compounds are isostructural, both crystallizing in the orthorhombic space group $Pna2_1$; their structures consist of novel 1D borophosphate chains constructed from $B_2P_3O_{14}$ fundamental building units, assembled into a 3D framework by alkali metal cations. Second-harmonic generation (SHG) measurements show that **1** and **2** are type-I phase-matchable, with SHG responses ca. 0.35 and 0.42 times that of KH_2PO_4, respectively. The cutoff edges of **1** and **2** are ca. 276 and 267 nm, respectively, which suggest that they are potential ultraviolet nonlinear optical materials. Density functional theory calculations were employed to shed light on the band structure and density of states as well as the electron density distribution.

Introduction

Nonlinear optical (NLO) crystals possessing ultraviolet (UV) frequency conversion activity are increasingly important because of rapid developments in UV laser science and technology.[1-5] Various high performance UV NLO-active crystals such as β-BaB_2O_4 (BBO),[6] LiB_3O_5 (LBO),[7] $Li_4Sr(BO_3)_2$,[8] $Ba_3(ZnB_5O_{10})PO_4$,[9] $Ba_3P_3O_{10}Cl$,[10] and $RbMgPO_4{\cdot}6H_2O$[11] have been reported in the past years. One of recent research focuses in this field is borophosphates (with connected borates BO_3 or BO_4 and phosphates PO_4) associated with alkali/alkaline earth metals, such as $KSrBP_2O_8$,[12] $RbPbBP_2O_8$,[13] $SrBPO_5$,[14] and $BaBPO_5$[14], which are of great interest as a new type of NLO materials.

Borophosphates display a rich structural chemistry; various isolated species, infinite chains, sheets, and frameworks constructed from complex anionic groups built of BO_3, BO_4, and PO_4 tetrahedra have been reported.[15,16] Alkali/alkaline-earth metal atoms can convert the 3D anionic frameworks into low dimensional structures. For example, $KMBP_2O_8$ (M = Sr, Ba)[12] and $Li_3Cs_2M_2B_3P_6O_{24}$ (M = Pb, Sr)[17] possess 3D B–P–O frameworks, $Li_2Cs_2B_2P_4O_{15}$,[18] $LiK_2BP_2O_8$,[18] and $Li_3M_2BP_4O_{14}$ (M = K, Rb)[18] exhibit 2D B–P–O layer structures, $MBPO_5$ (M = Ba, Sr)[14] and $Li_3BP_2O_8$[19] have 1D B–P–O chain structures, and $K_7B_2P_5O_{19}$[20] exhibits isolated B–P–O groups. However, to the best of our knowledge, there is no report of NLO properties of mixed-alkali-metal borophosphates with 1D B–P–O chain structures thus far.

Several different approaches have been employed to synthesize borophosphates. Hydrothermal methods have been widely used to control the growth of novel borophosphates;[21-23] although the hydrothermal procedure can produce well-defined crystals easily, OH^- and/or H_2O in the hydrated phases may have poor chemical and thermal stability and cause the UV cutoff edge of a crystal to red-shift.[24] High-temperature solid-state methods, have proven successful, affording a variety of acentric structures with second-harmonic generation (SHG) responses, such as $MPbBP_2O_8$ (M = K, Rb)[13,25], $Na_3Cd_3B(PO_4)_4$,[26] and β-Zn_3BPO_7;[27] although the high-temperature procedure can produce well-defined crystals, it requires lengthy reactions and often forms glassy products. Low-temperature flux methods have also afforded a variety of anhydrous borophosphates,[28,29] however, the use of this facile synthetic procedure to grow NLO-active borophosphates crystals is unreported to date.

We report herein the synthesis of two mixed-alkali-metal anhydrous borophosphates, $Na_4MB_2P_3O_{13}$ (M = Rb **1**, Cs **2**), the first examples of SHG-active metal borophosphate crystals, via

[a] China-Australia Joint Research Center for Functional Molecular Materials, School of Chemical and Material Engineering, Jiangnan University, Wuxi 214122, P. R. China.
[b] China-Australia Joint Laboratory for Functional Molecules and Ordered Matter, School of Chemical Science and Engineering, Tongji University, 200092, P. R. China. Email: chizhang@tongji.edu.cn
[c] Key Laboratory of Materials for High-Power Laser, Shanghai Institute of Optics and Fine Mechanics, Chinese Academy of Sciences, Shanghai 201800, P. R. China. E-mail: czhang@siom.ac.cn
[d] China-Australia Joint Research Center for Functional Molecular Materials, Jiangsu University, Zhenjiang 212013, P. R. China
[e] Research School of Chemistry, Australian National University, Canberra, ACT 2601, Australia.

† Electronic Supplementary Information (ESI) available: X-ray crystallographic file in CIF format (CCDC-1563595 for **1** and CCDC-1563594 for **2**), additional structures, selected bond distances and angles, simulated and measured powder XRD patterns, IR spectra, TGA and band structures. For ESI and crystallographic data in CIF or other electronic format see DOI: 10.1039/x0xx00000x

the facile low-temperature flux methods. The crystal structures, thermal stabilities, UV-Vis-NIR diffuse reflectance spectra, and SHG properties with a short cutoff edge and good phase-matchability for compounds **1** and **2** are also described in this paper. Theoretical studies on both compounds employing density functional theory (DFT) methods have been undertaken to explore the influence of the alkali metal substitution on the SHG properties.

Experimental

Reagents

Cs_2CO_3 (99%), Rb_2CO_3 (99.9%), NaF (99%), H_3BO_3 (99.5%) and $(NH_4)(H_2PO_4)$ (99.5%) were obtained commercially and used as received.

Synthesis of $Na_4RbB_2P_3O_{13}$ (1)

A mixture of Rb_2CO_3 (0.461 g, 2.00 mmol), NaF (0.082 g, 2.00 mmol), H_3BO_3 (0.183 g, 3.00 mmol) and $(NH_4)(H_2PO_4)$ (0.345 g, 3.00 mmol) was sealed in a 20 mL autoclave equipped with a Teflon liner. The autoclave was heated at 220 °C for 96 h, and then slowly cooled to 30 °C at 4 °C/h. After washing with deionized water, colorless block crystals of **1** were isolated using a microscope (0.092 g, 37% based on Na). IR data (KBr pellet, cm^{-1}): 1184 m, 1141 m, 1101 m, 1018 m, 960 m, 945 m, 826 m, 756 w, 622 w, 543 m.

Synthesis of $Na_4CsB_2P_3O_{13}$ (2)

The same procedure was employed to synthesize **2** except using Cs_2CO_3 (0.651 g, 2.00 mmol) instead of Rb_2CO_3. Colorless block crystals of $Na_4CsB_2P_3O_{13}$ (**2**) were obtained (0.186 g, 68% based on Na). IR data (KBr, pellet, cm^{-1}): 1183 m, 1142 m, 1100 m, 1018 m, 961 m, 943 m, 826 m, 757 w, 620 w, 543 m.

Structural Determinations

Single-crystal X-ray diffraction data of **1** and **2** were collected at room temperature on a Bruker D8 VENTURE CMOS X-ray diffractometer using graphite-monochromated Mo-$K\alpha$ radiation (λ = 0.71073 Å). APEX II software was applied to collect and reduce data. Semi-empirical absorption corrections based on equivalent reflections were applied for both data sets using the APEX II program. The two structures were solved by direct methods and refined on F^2 by full-matrix least-squares methods using SHELXTL.[30a,30b] All non-hydrogen atoms were refined anisotropically. The structures were checked with PLATON, and no other higher symmetry elements were found.[30c] Table 1 summarizes the crystal data and structural refinement parameters for the two compounds. Selected bond distances (Å) and angles (deg) are collected in Table S1 and Table S2 (Supporting Information).

Powder XRD

Table 1. Crystallographic Data and Structure Refinement Parameters for **1** and **2**.

Empirical formula	$Na_4RbB_2P_3O_{13}$	$Na_4CsB_2P_3O_{13}$
Formula weight	499.96	547.40
Temperature (K)	293(2)	293(2)
Crystal system	orthorhombic	orthorhombic
Space group	$Pna2_1$	$Pna2_1$
a (Å)	24.0348(9)	24.5034(9)
b (Å)	6.7464(2)	6.7673(2)
c (Å)	14.9206(6)	14.7803(5)
α (°)	90	90
β (°)	90	90
γ (°)	90	90
Volume ($Å^3$)	2419.35(15)	2450.90(14)
Z	8	8
Density (Calculated) ($g \cdot cm^{-3}$)	2.745	2.967
Absorption coefficient (mm^{-1})	4.705	3.626
F(000)	1919	2064
Theta range for data collection (°)	3.14-26.37	3.12-27.08
Limiting indices	$-27 \leqslant h \leqslant 30$, $-8 \leqslant k \leqslant 8$, $-17 \leqslant l \leqslant 18$	$-30 \leqslant h \leqslant 31$, $-8 \leqslant k \leqslant 8$, $-18 \leqslant l \leqslant 18$
R_{int}	0.0327	0.0274
Reflections collected/unique	13216/4830	14138/4997
Goodness-of-fit on F^2	1.071	1.098
Final R indices [$F_o^2 > 2\sigma(F_o^2)$][a]	0.0432/0.1113	0.0282/0.0609
R indices (all data) [a]	0.0545/0.1194	0.0346/0.0635
Largest diff. peak and hole (e. $Å^{-3}$)	0.826 and -1.456	0.558 and -0.998

[a] $R_1 = \sum ||F_o| - |F_c|| / \sum |F_o|$; $wR_2 = [\sum w(F_o^2 - F_c^2)^2] / \sum w(F_o^2)^2]^{1/2}$

Powder XRD data of **1** and **2** were recorded on a Bruker D8 X-ray diffractometer equipped with Cu-Kα radiation (λ = 1.5418 Å) in the angular range 2ϑ = 5–70° with a scan step-width of 0.02°.

IR Spectra

The IR spectra were measured on a Nicolet 360 FT-IR instrument within the range 500–4000 cm^{-1}. The samples were mixed thoroughly with dried KBr and were then pressed into discs for measurements.

UV-Vis-NIR Diffuse Reflectance Spectra

Optical diffuse-reflectance spectra were measured at room temperature with a UV-3600 Plus UV-Vis-NIR spectrophotometer. $BaSO_4$ was used as standard. Reflectance spectra were converted into absorbance based on the Kubelka–Munk function.[31]

Thermal Analysis

A TGA/1100SF instrument was used to analyze the thermal stabilities of the two compounds. The samples were heated from 50 °C to 900 °C with a heating rate of 10 °C/min in nitrogen gas.

Second-Order NLO Measurements

The powder SHG response of samples **1** and **2** was investigated using the Kurtz and Perry method.[32] A Q-switched Nd:YAG laser with 1064 nm radiation was employed for visible SHG. Because the SHG efficiency depends on particle size, compounds **1** and **2** were ground and sieved into several particle sizes (<26, 26−50, 50−74, 74−105, 105−150 and 150−200 μm), which were pressed into disks with diameters of 6 mm that were placed between glass microscope slides and secured with tape in a 1 mm thick aluminum holder. Crystalline KDP was also ground and sieved into the same particle size ranges and used as the reference.

Calculation Details

All electronic structure calculations were performed using the VASP code[33a] within the framework of density functional theory (DFT). The generalized gradient approximation (GGA) function of Perdew-Burke-Ernzerhof (PBE)[33b] was employed. A plane-wave basis set with a frozen-core projector-augmented wave (PAW)[33c,33d] potential and a plane-wave cutoff energy of 400 eV were used. A grid of 5 × 5 × 4 Monkhurst-Pack *k*-points was used for the self-consistent-field convergence of the total electronic energy. The Fermi level was set at zero as the energy reference.

Results and discussion

Syntheses

Previous preparations of anhydrous metal borophosphates were conducted at either high temperatures (> 600 °C) or high pressures (> 100 bar) (e.g. $CsFe(BP_3O_{11})$,[34] $Cs_2Cr_3(BP_4O_{14})(P_4O_{13})$,[34] $BiCo_2BP_2O_{10}$,[35] $BiNi_2BP_2O_{10}$,[35] $Li_2B_3PO_8$[36]). The conventional high-temperature solid-state reactions also have afforded a wide variety of alkali/alkaline-earth metal borophosphates with good second-order NLO properties, such as $KSrBP_2O_8$ (0.2 × KDP, λ = 313 nm),[12] $RbPbBP_2O_8$ (1.0 × KDP, λ = 280 nm),[13] $BaBPO_5$ (0.43 × KDP, λ = 202 nm),[14] and $SrBPO_5$ (0.57 × KDP, λ = 193 nm).[14] In contrast to extant NLO-active borophosphates that were prepared under forcing conditions, we adopted a milder and more energy-efficient method, low-temperature flux reaction, using Rb_2CO_3/Cs_2CO_3, NaF, H_3BO_3 and $(NH_4)(H_2PO_4)$ as the starting materials and reaction at 220 °C. Since boric acid melts as low as 171 °C, excess boric acid is a suitable medium for flux synthesis for borophosphates.[15] This synthetic procedure afforded the two UV SHG-active mixed-alkali-metal borophosphates without OH^- or H_2O, $Na_4MB_2P_3O_{13}$ (M = Rb **1**, Cs **2**), exhibiting good thermal stability and wide UV transparency.

Crystal Structures

Single-crystal X-ray diffraction analysis revealed that the two mixed-alkali-metal borophosphate crystals $Na_4MB_2P_3O_{13}$ (M = Rb **1**, Cs **2**) are isostructural, both crystallizing in the orthorhombic crystal system with achiral nonpolar space group

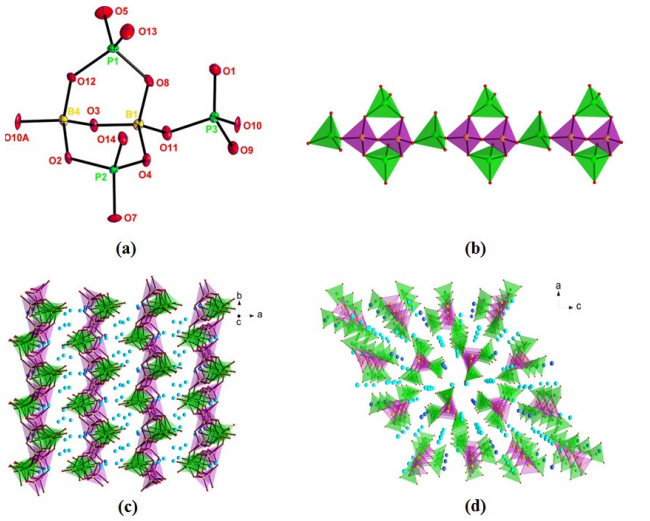

Figure 1. (a) $B_2P_3O_{14}$ cluster unit. Symmetry code: (A) x, 1 + y, z. (b) View of the infinite chain constructed from the $B_2P_3O_{14}$ units. (c) Structure of **2** viewed along the *c*-axis. (d) Perspective view of the 3D structure of **2** projected along the *b*-axis. The Na–O and Cs–O bonds have been omitted for clarity. Color codes: B gold, P, green, O red, Na turquoise, Cs light blue, PO_4 tetrahedron green, BO_4 tetrahedron purple.

$Pna2_1$ (No. 33); as a result, only a representative structure, that of crystal **2**, will be discussed in detail.

In the structure of **2**, the fundamental building unit (FBU), $B_2P_3O_{14}$ (B/P = 2:3), is comprised of two BO_4 and three PO_4 units (Figure 1a). Each $B_2P_3O_{14}$ FBU is attached to adjacent FBUs by sharing common O(10) or O(25) atoms, thereby forming 1D infinite chains along the *b*-axis (Figure 1b).

The asymmetric unit of **2** contains 8 Na, 2 Cs, 4 B, 6 P and 26 O atoms (Figure S1, Supporting Information). Each B atom is coordinated by four oxygen atoms, forming a nearly ideal BO_4 tetrahedral geometry. Atoms B(3) are located on the two-fold axis. The B–O bond lengths and O–B–O bond angles are in the range 1.416(6)–1.520(7) Å and 103.5(4)–115.5(4)° in the BO_4 tetrahedra, respectively. Each P atom is tetrahedrally coordinated by four O atoms with P–O bond lengths and O–P–O bond angles ranging from 1.481(6)–1.584(4) Å and 101.8(2)–116.4(4)°, respectively. These values are comparable to those of previously reported borophosphate compounds.[37]

There are two types of Na atoms in **2**, one type coordinated to 5 O atoms and the other to 6 O atoms, with Na–O distances in the range 2.214(5)–2.968(4) Å (Figure S2, Supporting Information). The Cs atoms are bonded to 13 O atoms with Cs–O distances in the range 3.075(4)–3.784(4) Å. The Na^+ and Cs^+ cations provide the compensating positive charges in the structure and are located between adjacent polyborate chains (Figure 1c), which assemble into a 3D framework linked by the Na-O and Cs-O bonds (Figure 1d). Bond valence calculations (Na, 0.89–1.22; Cs, 0.67–0.78; B 3.03–3.09; P 4.79–4.93) are consistent with oxidation states of +1 for Na, +1 for Cs, +3 for B, and +5 for P, respectively. The difference between the isostructural **1** and **2** lies in the coordination modes of the Cs^+ and the Rb^+ cations. As mentioned above, the Na atoms in **1** are coordinated by five or six O atoms (Na–O: 2.225(5)–

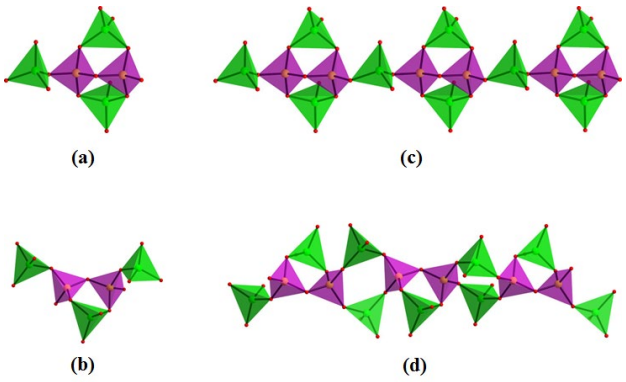

Figure 2. (a) $[B_2P_3O_{14}]$ (5□:<3□>=<3□>□) FBU in **2**. (b) $[B_2P_3O_{14}]$ (5□:□<3□>□) FBU in $[Co(en)_3][B_2P_3O_{11}(OH)_2]$. The infinite borophosphate chains in (c) **2**, and (d) $[Co(en)_3][B_2P_3O_{11}(OH)_2]$. Symbol □ represents BO_4 and PO_4 tetrahedra. The green and purple tetrahedra represent the PO_4 and BO_4 units, respectively.

2.947(8) Å), whereas the Rb atoms in **1** are surrounded by nine and ten O atoms with Rb–O bond distances ranging from 2.945(7) Å to 3.582(7) Å.

We compared the anionic structure of **2** with that of $[Co(en)_3][B_2P_3O_{11}(OH)_2]$[38] as they have the same B/P toichiometry. The FBU of the anionic partial structures in the borophosphates is an important classification criteria.[16] Although compound **2** and $[Co(en)_3][B_2P_3O_{11}(OH)_2]$ have the same B/P ratio, they exhibit different FBUs. The FBU of **2**, $[B_2P_3O_{14}]$, can be written as 5□:<3□>=<3□>□ while the FBU of $[Co(en)_3][B_2P_3O_{11}(OH)_2]$ can be represented as 5□:□<3□>□ (Figures 2a and 2b). These two compounds thus display distinctly different anionic chain structures (Figures 2c and 2d).

Powder XRD patterns of **1** and **2** were also obtained (Figure S3, Supporting Information); there is a good match between the experimental powder XRD patterns of the two samples and the calculated ones derived from the single-crystal data, confirming bulk homogeneity of these materials.

IR Measurements

The infrared spectra of **1** and **2** are shown in Figure S4 (Supporting Information), and are comparable with reported metal borophosphates.[17] The bands around 1184, 1140, 960 cm^{-1} are the characteristic of tetrahedral PO_4 groups, while the bands at 1100 and 945 cm^{-1} can be assigned to the BO_4 groups. The split peaks result from small distortions of the PO_4 and BO_4 tetrahedra. The absorption bands around 725–845 cm^{-1} can be attributed to asymmetric and symmetric stretching vibrations of B–O–P groups. The bending vibrations of O–P–O, B–O–B and B–O–P groups are observed between 500 and 700 cm^{-1}.

UV-Vis-NIR Diffuse Reflectance Spectra

The UV-Vis-NIR diffuse reflectance spectra for **1** and **2** are shown in Figure 3. Absorption data were calculated employing the Kubelka–Munk function: $F(R) = (1-R)^2/2R = K/S$. **1** and **2** have wide band-gap energies of 4.50 and 4.65 eV with cutoff

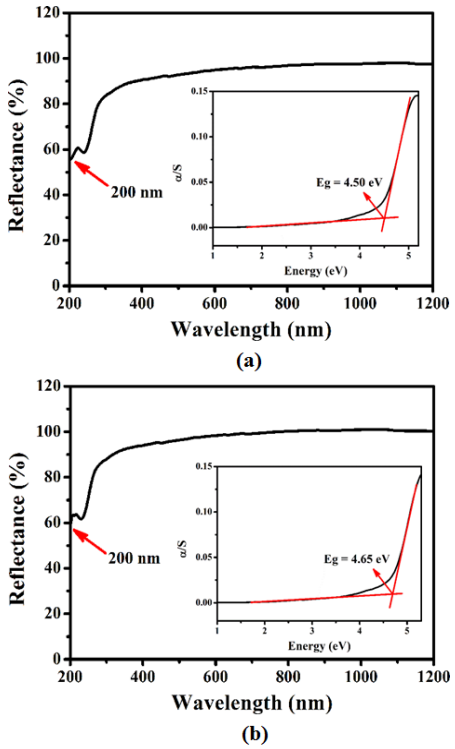

Figure 3. UV-Vis-NIR diffuse reflectance spectra of **1** (a) and **2** (b). The inserts show the corresponding band gaps.

edges of 276 and 267 nm, respectively. These UV cutoff edge values are a little bit shorter than those of other reported metal borophosphates, such as $KSrBP_2O_8$ (3.97 eV),[12] $RbPbBP_2O_8$ (4.42 eV),[13] $Li_3Cs_2Sr_2B_3P_6O_{24}$ (3.70 eV),[17] $Na_3Cd_3B(PO_4)_4$ (3.44 eV),[26] $LiPb_4(BO_3)(PO_4)_2$ (3.54 eV).[39] The wide transparency range (from the UV to the NIR) and short wavelength cutoff edges of **1** and **2** indicate that these two mixed-alkali-metal borophosphate crystals are potential UV NLO materials.

Thermal Stabilities

The thermal behaviors of **1** and **2** are almost the same (Figure S5, Supporting Information). As shown in the thermogravimetric analysis (TGA) curves, both compounds are thermally stable up to high temperatures with nearly no weight loss. Only one endothermic peak is observed in the heating curves of the differential scanning calorimetry (DSC) results (707 and 741 °C for compounds **1** and **2**, respectively).

SHG Properties

Since **1** and **2** crystallize in the acentric space group $Pna2_1$, we were encouraged to study their SHG properties. The powder NLO properties of the title compounds were systematically studied as a function of particle size with a Q-switched Nd:YAG laser (1064 nm). The SHG intensities of **1** and **2** increase with increasing particle size before they reach a maximum that is independent of particle size (Figure 4a), consistent with phase-matchable behavior. With the same particle size range of

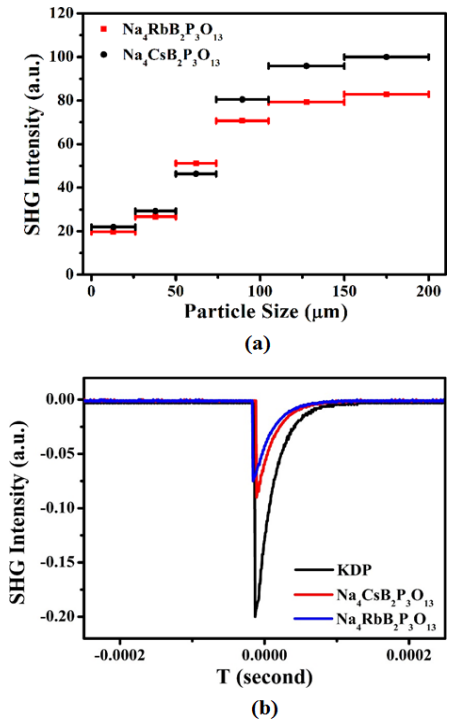

Figure 4. (a) Phase-matchable curves of **1** and **2** with 1064 nm laser radiation. (b) Oscilloscope traces of the SHG signals for powders of **1**, **2** and KDP in the same particle size range of 105-150 μm.

105−150 μm, the SHG efficiencies of **1** and **2** are 0.35 and 0.42 times that of KDP, respectively (Figure 4b). These values are comparable to those reported for other metal borophosphates, e.g. $BaBPO_5$ (0.4 × KDP),[14] $SrBPO_5$ (0.6 × KDP),[14] $KSrBP_2O_8$ (0.2 ×KDP)[12] and $KBaBP_2O_8$ (0.33 × KDP)[12]. According to anionic group theory, the overall SHG response of the crystal is the geometrical superposition of the microscopic second-order susceptibility.[40] In the structures of **1** and **2**, the BO_4 and PO_4 tetrahedra only possess a small microscopic second-order susceptibility. In addition, the linkage modes of the tetrahedral groups in adjacent chains are opposite along *b*-axis, which are not favorable to generate the large SHG effects. This is consistent with the experimental results of SHG measurements of **1** and **2** in this study.

Theoretical Calculations

To gain further insight into the electronic structures of **1** and **2**, theoretical calculations of the compounds were performed using DFT methods. The band structures (Figure S6, Supporting Information) show that **1** and **2** are indirect band-gap compounds, because the valence band maximum (VBM) and the conduction band minimum (CBM) are at different points (Y and Γ, respectively). The minimum optical band gaps were calculated to be 5.02 eV for **1** and 5.10 eV for **2**; these values are larger than the experimental optical band gaps, which may be due to the fact that strong excitonic effects[41] exist in these compounds.[17,42]

The electron densities of the VBMs and CBMs for **1** and **2** are given in Figure 5. The VBMs of the two compounds consist of O 2p states localized at the O atom, while the CBMs are significantly delocalized and largely composed of states from the Cs^+ or Rb^+ cations and the $[PO_4]^{3-}$ units. The electron density of oxygen in the VBM of **1** is slightly larger than that of

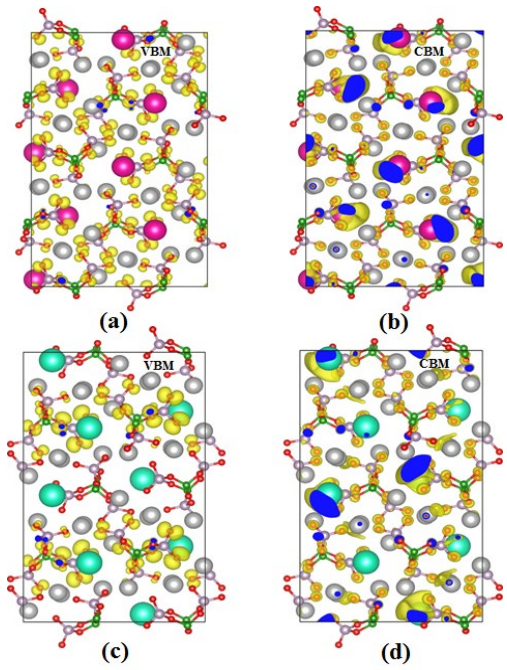

Figure 5. Electron density of the valence band maximal (VBM, (a), (c)) and conduction band minimal (CBM, (b), (d)) for **1** (top) and **2** (bottom). The isosurface value is set to 0.001 eV/Å^3. red: oxygen; green: boron; light pink: phosphorus; gray: sodium; pink: rubidium; turquoise: caesium.

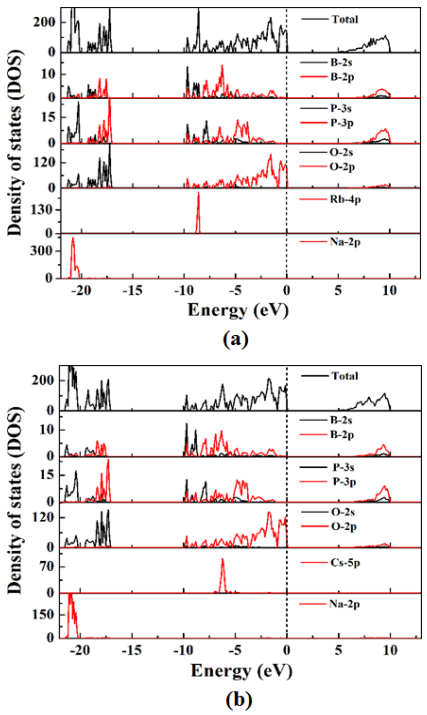

Figure 6. Total density of states (DOS) and partial density of states (PDOS) of **1** (a) and **2** (b); Fermi levels (dotted lines) located at zero.

2, while the electron density of oxygen in the CBM for the two compounds is similar, indicating that charge-transfer from the CBM to the VBM in compound **2** is larger than that of **1**, or, in other words, the electronic polarization in compound **2** is larger than that of **1**. Because the nonlinear responses of materials are closely related to their electronic polarizabilities, the calculations suggest (and this is borne out by experiment) that **2** shows a slightly larger SHG efficiency than **1**.

The density of states (DOS) plots for the two compounds are quite similar (Figure 6). The Na orbitals are mainly distributed deep in the valence band (VB) (←20 eV) and far from the Fermi level, and they have very little overlap with the neighboring atoms. As a result, their contribution to the optical nonlinearity in both compounds can be ignored. The upper region of the VB (-10 to 0 eV) is predominantly derived from Rb 4p/Cs 5p, B 2p, P 3p, and O 2p orbitals. A significant hybridization of the B 2p, P 3p and O 2p states is observed, indicating that the major contribution to the VB maximum originates from the B–O and P–O bonds. The lower energy region of the conduction band (CB) (0–10 eV) is mostly composed of B 2p and P 3p states. Based on this analysis, we conclude that the BO_4 and PO_4 anionic groups determine the energy band gaps and optical properties of the two compounds, although the effect of the Rb^+/Cs^+ cations cannot be ignored.

Conclusions

In summary, two novel achiral nonpolar borophosphates, $Na_4MB_2P_3O_{13}$ (M = Rb **1**, Cs **2**), have been synthesized by a facile low-temperature flux method. Compounds **1** and **2** are isostructural, consisting of $B_2P_3O_{14}$ FBUs and featuring 1D anionic chains. The alkali-metal counter-ions are located around the chains and linked by metal–oxygen bonds, affording a 3D framework. These compounds exhibit SHG response (0.35 × KDP for **1** and 0.42 × KDP for **2**) at 1064 nm and short UV cutoff edges (276 nm for **1** and 267 nm for **2**), and are phase-matchable in the visible region. These features make **1** and **2** potential UV NLO materials. Further research developing borophosphates under low-temperature flux conditions for UV NLO materials is currently in progress.

Acknowledgements

This research was financially supported by the National Natural Science Foundation of China (no. 51432006, 50925207, and 51172100), the Ministry of Science and Technology of China (no. 2011DFG52970), the Ministry of Education of China for the Changjiang Innovation Research Team (no. IRT13R24), and the Ministry of Education and the State Administration of Foreign Experts Affairs for the 111 Project (no. B13025). M. G. H. and C. Z. thank the Australian Research Council for support.

Notes and references

1 (a) M. Lee, H. E. Katz, C. Erben, D. M. Gill, P. Gopalan, J. D. Heber, D. J. McGee, *Science*, 2002, **298**, 1401; (b) D. Cyranoski, *Nature*, 2009, **457**, 953; (c) N. Savage, *Nature Photon.*, 2007, **1**, 83.

2 (a) T. T. Tran, H. W. Yu, J. M. Rondinelli, K. R. Poeppelmeier, P. S. Halasyamani, *Chem. Mater.*, 2016, **28**, 5238; (b) C. Q. Zhu, Z. T. Lei, L. C. Song, T. H. Ma, C. H. Yang, *J. Cryst. Growth*, 2015, **421**, 53; (c) T. C. Lin, J. M. Cole, A. P. Higginbotham, A. J. Edwards, R. O. Piltz, J. Perez-Moreno, J. Y. Seo, S. C. Lee, K. Clays, O. P. Kwon, *J. Phys. Chem. C*, 2013, **117**, 9416.

3 (a) L. Li, Y. Wang, B. H. Lei, S. J. Han, Z. H. Yang, K. R. Poeppelmeier, S. L. Pan, *J. Am. Chem. Soc.*, 2016, **138**, 9101; (b) P. Yu, L. M. Wu, L. J. Zhou, L. Chen, *J. Am. Chem. Soc.*, 2014, **136**, 480; (c) S. G. Zhao, P. F. Gong, S. Y. Luo, L. Bai, Z. S. Lin, Y. Y. Tang, Y. L. Zhou, M. C. Hong, J. H. Luo, *Angew. Chem. Int. Ed.*, 2015, **54**, 4217; (d) L. Li, S. J. Han, B. H. Lei, Y. Wang, H. Y. Li, Z. H. Yang, S. L. Pan, *Dalton Trans.*, 2016, **45**, 3936; (e) E. R. Wang, J. H. Huang, S. J. Yu, Y. Z. Lan, J. W. Cheng, G. Y. Yang, *Inorg. Chem.*, 2017, **56**, 6780. (d) Z. H. Li, Z. S. Lin, Y, C. Wu, P. Z. Fu, Z. Z. Wang, C. T. Chen, *Chem. Mater.*, 2004, **16**, 2906.

4 (a) T. T. Tran, H. W. Yu, J. M. Rondinelli, K. R. Poeppelmeier, P. S. Halasyamani, *Chem. Mater.*, **2016**, *28*, 5238; (b) G. H. Zou, N. Ye, L. Huang, X. S. Lin, *J. Am. Chem. Soc.*, 2011, **133**, 20001; (c) Y. X. Song, M. Luo, C. S. Lin, N. Ye, *Chem. Mater.*, 2017, **29**, 896; (d) L. Huang, G. H. Zou, H. Q. Cai, S. C. Wang, C. S. Lin, N. Ye, *J. Mater. Chem. C*, 2015, **3**, 5268; (e) J. H. Jiang, L. C. Zhang, Y. X. Huang, Z. M. Sun, Y. M. Pan, J. X. Mi, *Dalton Trans.*, 2017, **46**, 1677.

5 (a) C. Wu, L. H. Li, J. L. Song, G. Yang, M. G. Humphrey, C. Zhang, *Inorg. Chem. Front.*, 2017, **4**, 692; (b) C. Wu, L. H. Li, J. L. Song, G. Yang, M. G. Humphrey, C. Zhang, *Inorg. Chem.*, 2017, **56**, 1340; (c) C. Wu, J. L. Song, L. H. Li, M. G. Humphrey, C. Zhang, *J. Mater. Chem. C*, 2016, **4**, 8189.

6 C. T. Chen, B. C. Wu, A. D. Jiang, G. M. You, *Sci. Sin., Ser. B*, 1985, **28**, 235.

7 C. T. Chen, Y. C. Wu, A. D. Jiang, B. C. Wu, G. M. You, R. K. Li, S. J. Lin, *J. Opt. Soc. Am. B*, 1989, **6**, 616.

8 S. G. Zhao, P. F. Gong, L. Bai, X. Xu, S. Q. Zhang, Z. H. Sun, Z. S. Lin, M. C. Hong, C. T. Chen, J. H. Luo, *Nature Commun.*, 2014, **5**, 4019.

9 H. W. Yu, W. G. Zhang, J. H. Young, J. M. Rondinelli, P. S. Halasyamani, *Adv. Mater.*, 2015, **27**, 7380.

10 P. Yu, L. M. Wu, L. J. Zhou, L. Chen, *J. Am. Chem. Soc.*, 2014, **136**, 480.

11 Y. Q. Zhou, L. L. Cao, C. S. Lin, M. Luo, T. Yan, N. Ye, W. D. Cheng, *J. Mater. Chem. C*, 2016, **4**, 9219.

12 D. Zhao, W. D. Cheng, H. Zhang, S. P. Huang, Z. Xie, W. L. Zhang, S. L. Yang, *Inorg. Chem.*, 2009, **48**, 6623.

13 Y. Wang, S. L. Pan, M. Zhang, S. J. Han, X. Su, L. Y. Dong, *CrystEngComm*, 2013, **15**, 4956.

14 B. H. Lei, Q. Jing, Z. H. Yang, B. B. Zhang, S. L. Pan, *J. Mater. Chem. C*, 2015, **3**, 1557.

15 M. Li, A. Verena-Mudring, *Cryst. Growth Des.*, 2016, **16**, 2441.

16 B. Ewald, Y. X. Huang, R. Kniep, *Z. Anorg. Allg. Chem.*, 2007, **633**, 1517.

17 (a) L. J. Zhang, Y. Y. Li, P. F. Liu, L. Chen, *Dalton Trans.*, 2016, **45**, 7124. (b) A. Baykal, G. Gözel, M. Kizilyalli, *Turk. J. Chem.*, 2000, **24**, 381.

18 Y. Wang, S. L. Pan, Y. J. Shi, *Chem. Eur. J.*, 2012, **18**, 12046.

19 T. Hasegawa, H. Yamane, *Dalton Trans.*, 2014, **43**, 2294.

20 Y. Wang, S. L. Pan, S. J. Han, B. B. Zhang, L. Y. Dong, M. Zhang, Z. H. Yang, *CrystEngComm*, 2014, **16**, 6848.

21 S. Hoffmann, H. B. T. Jeazet, P. W. Menezes, Y. Prots, R. Kniep, *Inorg. Chem.*, 2008, **47**, 10193.

22 W. T. Yang, J. Y. Li, Q. H. Pan, H. Z. Xing, Y. Chen, J. H. Yu, R. R. Xu, *J. Mater. Chem.*, 2009, **19**, 4523.
23 Y. Feng, M. Li, H. Shi, Q. Huang, D. Qiu, *CrystEngComm*, 2013, **15**, 2048.
24 C. D. McMillen, J. T. Stritzinger, J. W. Kolis, *Inorg. Chem.* **2012,** *51*, 3953.
25 H. Y. Li, Y. Zhao, S. L. Pan, H. P. Wu, H. W. Yu, F. F. Zhang, Z. H. Yang, K. R. Poeppelmeier, *Eur. J. Inorg. Chem.*, 2013, **18**, 3185.
26 Y. J. Shi, S. L. Pan, X. Y. Dong, Y. Wang, M. Zhang, F. F. Zhang, Z. X. Zhou, *Inorg. Chem.*, 2012, **51**, 10870.
27 G. Wang, Y. Wu, P. Fu, X. Liang, Z. Xu, C. Chen, *Chem. Mater.*, 2002, **14**, 2044.
28 D. B. Xiong, H. H. Chen, X. X. Yang, J. T. Zhao, *J. Solid State Chem.*, 2007, **180**, 233.
29 S. J. Wu, M. J. Polinski, T. Malcherek, U. Bismayer, M. Klinkenberg, G. Modolo, D. Bosbach, W. Depmeier, T. E. Albrecht-Schmitt, E. V. Alekseev, *Inorg. Chem.*, 2013, **52**, 7881.
30 (a) G. M. Sheldrick, *SHELXS-97: Program for the Solution of Crystal Structures*; University of Göttingen, Germany, 1997; (b) G. M. Sheldrick, *SHELXL-97: Program for the Refinement of Crystal Structures*; University of Göttingen, Germany, 1997; (c) A. L. Spek, *PLATON*; Utrecht University: Utrecht, The Netherlands, 2001.
31 W. M. Wendlandt, H. G. Hecht, *Reflectance Spectroscopy*; Interscience: New York, 1966.
32 S. K. Kurtz, T. T. Perry, *J. Appl. Phys.*, 1968, **39**, 3798.
33 (a) G. Kresse, J. Furthmuller, *Phys. Rev. B*, 1996, **54**, 11169; (b) J. P. Perdew, K. Burke, M. Ernzerhof, *Phys. Rev. Lett.*, 1996, **77**, 3865; (c) P. E. Blochl, *Phys. Rev. B*, 1994, **50**, 17953; (d) G. Kresse, D. Joubert, *Phys. Rev. B*, 1999, **59**, 1758.
34 W. Zhang, W. Cheng, H. Zhang, L. Geng, Y. Li, C. Lin, Z. He, *Inorg. Chem.*, 2010, **49**, 2550.
35 W. L. Zhang, Z. Z. He, T. L. Xia, Z. Z. Luo, H. Zhang, C. S. Lin, W. D. Cheng, *Inorg. Chem.*, 2012, **51**, 8842.
36 T. Hasegawa, H. Yamane, *Dalton Trans.*, 2014, **43**, 14525.
37 (a) W. Yang, J. Li, Q. Pan, Z. Jin, J. Yu, R. Xu, *Chem. Mater.*, 2008, **20**, 4900. (b) S. Wang, E. V. Alekseev, J. T. Stritzinger, W. Depmeier, T. E. Albrecht-Schmitt, *Inorg. Chem.*, 2010, **49**, 6690.
38 G. Y. Yang, S. C. Sevov, *Inorg. Chem.*, 2001, **40**, 2241.
39 S. S. Huang, H. W. Yu, J. Han, S. L. Pan, Q. Jing, Y. Wang, L. Y. Dong, H. P. Wu, Z. H. Yang, X. Wang, *Eur. J. Inorg. Chem.*, 2014, **22**, 3467.
40 (a) C. T. Chen, *Sci. Sin. (Engl. Ed.)*, 1979, **22**, 756; (b) C. T. Chen, G. Z. Liu, *Annu. Rev. Mater. Sci.*, 1986, **16**, 203; (c) C. T. Chen, Y. C. Wu, R. K. Li, *Int. Rev. Phys. Chem.*, 1989, **8**, 65.
41 L. H. Li, O. Y. Kontsevoi, A. J. Freeman, *Phys. Rev. B*, 2014, **90**, 195203.
42 P. Yu, L. J. Zhou, L. Chen, *J. Am. Chem. Soc.*, 2012, **134**, 2227.